Solar Energy 173 (2018) 120–125

Contents lists available at ScienceDirect

Solar Energy

journal homepage: www.elsevier.com/locate/solener

Synthesis of sphere-like-crystal CdS powder and thin films using chemical residue in chemical bath deposition (CBD) for thin film solar cell application

Ameen M. Ali[a], Yulisa Yusoff[d], Lamya M. Ali[c], Halina Misran[d], Md. Akhtaruzzaman[a], Mohammad A. Alghoul[e], Kamaruzzaman Sopian[a], Shahidan Radiman[c], Nowshad Amin[a,b,d,*]

[a] Solar Energy Research Institute, The National University of Malaysia, Malaysia
[b] Faculty of Engineering and Built Environment, The National University of Malaysia, Malaysia
[c] Faculty of Science and Technology, The National University of Malaysia, Malaysia
[d] Institute of Sustainable Energy, Universiti Tenaga Nasional (@The National Energy University), Jalan IKRAM-UNITEN, 43000 Kajang, Selangor, Malaysia
[e] Center of Research Excellence in Renewable Energy (CoRERE), King Fahd University of Petroleum and Minerals, Dhahran 31261, Saudi Arabia

ARTICLE INFO

Keywords:
CBD
CdS
Residue
Thermal evaporation
Thin films

ABSTRACT

CdS microcrystal, with sphere like morphology, was synthesised from the residue obtained after the chemical bath deposition (CBD) of CdS thin layers usually deposited for CdTe and/or CIGS thin film solar cells, specifically by recycling the chemical waste. The residue was collected and reused to deposit cadmium sulphide (CdS) thin films on glass substrate by thermal evaporation. The films were subsequently annealed in vacuum at 250 °C, 350 °C and 420 °C for 40 min. The structural and optical properties were characterized by XRD, SEM, and UV–Vis spectrometry. All the films were found to exhibit high transmittance (over 70 to 90%). The optical band gap energy was found to be in the range of 2.28–2.37 eV, which is very suitable to be used as buffer or window for CdTe or CIGS thin film solar cells.

1. Introduction

Cadmium sulphide (CdS) is a group II-VI compound semiconductor material with a direct optical band gap of 2.482 eV at room temperature (Martienssen and Warlimont, 2006). It has high optical transmittance and ease of deposition making it very attractive for optoelectronic device applications. CdS grows intrinsically as n-type semiconductor (Richter et al., 2013; Oliva, 2001). CdS thin films are widely used in solar cells as the window layer in cadmium telluride (CdTe) recording efficiencies of 21.4% for cells and 17.5% for modules (Green, 2016). It is also used as buffer layer in copper indium gallium selenide, CuInGaSe$_2$)CIGS(based hetero-junction solar cells with efficiencies of 21.6% for cells and 18.7% for modules (Green, 2016; Chopra et al., 2004).

CdS buffer layer shows high window functionality for emerging new thin film PV technologies such as CZTS thin film solar cells with recent efficiencies 12.6% (Jean, 2015; Tao, 2016).

Several techniques have been used to deposit CdS thin films including chemical bath deposition (CBD) (Shah, 2012), sputtering (Lee and Lee, 2007), close spaced sublimation (CSS) (Ferekides, 2000), and thermal evaporation (Sahay et al., 2007). Even though the highest efficiency solar cells were fabricated using CdS by CBD, this technique is not suitable for large-scale production and involve a fairly slow process (Romeo, 2004). CBD also produces hazardous waste that needs to be recycled or safely disposed to safeguard the environment. Recovering or recycling the CdS from the CBD waste has many advantages from economic and environmental point of view.

In this work CdS crystal, with sphere-like morphology, was first synthesized using the chemical residue from CBD process, as the chemical bath deposition (CBD) waste was recycled. The prepared CdS crystal was used to deposit CdS thin films by low vacuum thermal evaporation method. Thermal evaporation is considered as a simple and low cost technique compared to other thin film deposition techniques. In window layer applications, it is desirable that the CdS layer should be as thin as possible (Morales-Acevedo, 2006), where preferable thickness is between (50–100) nm (Durose et al., 1999). In this work, CdS films with 50 nm and 60 nm thicknesses were obtained and characterized.

2. Methodology

Commercially available cadmium sulfate ($CdSO_4$), Thiourea ($SC(NH_2)_2$), ammonium hydroxide (NH_4OH), and ammonium sulfate

* Corresponding author at: Institute of Sustainable Energy, Universiti Tenaga Nasional (@The National Energy University), Jalan IKRAM-UNITEN, 43000 Kajang, Selangor, Malaysia.
E-mail address: nowshad@uniten.edu.my (N. Amin).

https://doi.org/10.1016/j.solener.2018.07.031
Received 6 June 2018; Accepted 10 July 2018
Available online 26 July 2018
0038-092X/

$(NH_4)_2SO_4$ were used without further purification (Sigma-Aldrich Co.). The deposition of CdS thin films was then carried out by chemical bath deposition (CBD) with the following the process. 0.002 M of $CdSO_4$, 0.006 M of$(NH_4)_2SO_4$was weighed and then mixed in the aqueous alkaline solution of NH_4OH and then 0.05 M of thiourea, SC $(NH_2)_2$ was added to the aqueous solutions and stirred constantly. The reaction temperature was controlled within the range of (338–353) K and the reaction time was set to 20–30 min. More details of the prepared CdS thin film using CBD method was discussed elsewhere (Yusoff, 2015). At the end of the process, the orange precipitate of CBD waste was collected. This precipitate was separated by centrifugation, washed several times with ethanol and distilled water, and then dried at 60 °C under vacuum overnight. The resultant CdS powder was used for preparing CdS thin films using thermal evaporation technique on cleaned soda lime glass substrate under low vacuum. The glass substrates used in the deposition were ultrasonically cleaned in acetone, ethanol, and de-ionized water successively and finally dried with N_2 before used.

Thermal evaporation is a simple technique for depositing material onto a substrate as thin films. It uses an electric resistance heater and has tungsten boat to heat the source material. The temperature of the boat increases with the increase in current eventually heating the source material which starts to evaporate. Hence, CdS is deposited using the thermal evaporation method and the entire process is done in low vacuum chamber allowing the molecules to evaporate freely in the chamber and they subsequently condense on the substrate as CdS thin films. The deposition parameters of CdS are mentioned in the following Table 1.

Thermally evaporated CdS thin films were annealed under vacuum at 250 °C, 350 °C, and 420 °C for 40 min, respectively. Table 2 summarizes the sample description for the CdS thin films that were annealed at different temperatures.

The structural investigation of CdS powder was carried out using X-ray powder diffractometer (Bruker AXS Germany, D8 Advance) with Cu - $K_\alpha$radiation wavelength λ = 1.5406 Å and angle (2θ = 20° to 60°) at room temperature. Grain size, surface morphology and cross-sectional view were observed by using Carl Zeiss Merlin field emission scanning electron microscope (FESEM) which was operated at 3 kV. The electrical parameters such as carrier concentration, mobility, and resistivity were measured by Hall Effect measurement system, HMS ECOPIA 3000 with a magnetic field of 0.57 T and UV–Vis spectrometry (Perkin-Elmer Lambad 35) in the wavelength range of 300 nm to 900 nm.

3. Results and discussion

Fig. 1 shows the attained cubic zinc-blende structure of CdS powder with space group *F-43m (2 1 6),* which was expected as it is commonly known that low temperature CBD CdS thin films were often found in cubic phase (Lisco, 2015; Mariappan, 2012). The peaks match to the JCPDS card numbered 01–0890440, where the peaks are associated with the (1 1 1), (2 2 0), and (3 1 1) planes.

The mean crystallite size (D) of CdS powder was also calculated using Scherrer equation as given in Eq. (1). The micro-strain (ε) was calculated from the XRD peaks using Eq. (2) (Guinebretière, 2013).

Table 1
Thermal evaporation deposition parameters.

Thermal Evaporation Parameters	Value/Range
Source	45 mg CdS recycled powder
Substrate	Soda lime glass
Boat to substrate distance	5 cm
Deposition current	25 A
Deposition Time	20 min
Deposition pressure	5 Pa

Table 2
Summary of annealing process parameters.

Sample ID	Annealing Temperature °C	Time of annealing min
As deposited	–	–
A	250	40
B	350	40
C	420	40

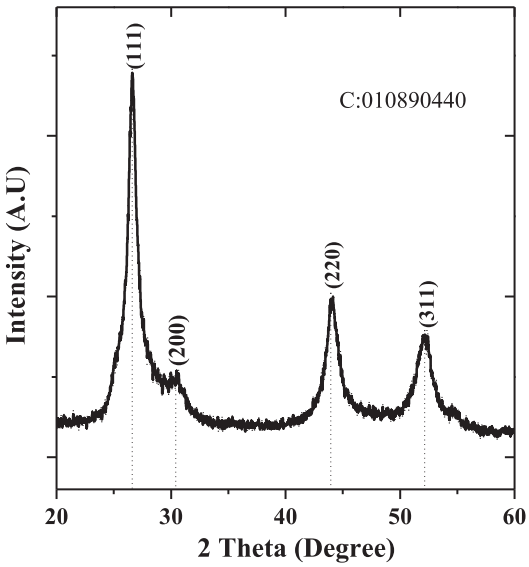

Fig. 1. XRD pattern of recycled CdS powder.

$$D = \frac{0.9\lambda}{\beta cos\theta} \quad (1)$$

$$\varepsilon = \frac{\beta}{4tan\theta} \quad (2)$$

where

D: the crystallite size,
λ: X-ray wavelength (1.54 Å),
β: Full width at half maximum (FWHM) (rad).

The crystallite size and micro-strain final calculations were done using the TOPAS (BrukerAXS, 2008) software. Results are summarised in Table 3 with goodness of fit (GOF = 1.31).

The corresponding lattice parameter of the CdS film as stated in the JCPDS card no. 01-0890440 is found to be a_0 = 5.80537 Å. The corresponding formulae for the lattice parameter of a cubic crystal system with inter-planar distance, *d*, is shown in Eq. (3). Using the formulae, the lattice parameter here was found to be a = 5.8295 Å (Pecharsky and Zavalij, 2009).

$$a^2 = d^2(h^2 + k^2 + l^2) \quad (3)$$

FESEM images in Fig. 2(a)–(d), show that CdS microstructure was

Table 3
Parameters from XRD calculation.

2° θ	Miller indices	Crystallite size (nm)	Microstrain ($\times 10^{-3}$)
26.6	)111(	26.4	17.5
44.1	(220(	54.4	14
52.1	(311)	87	15.5

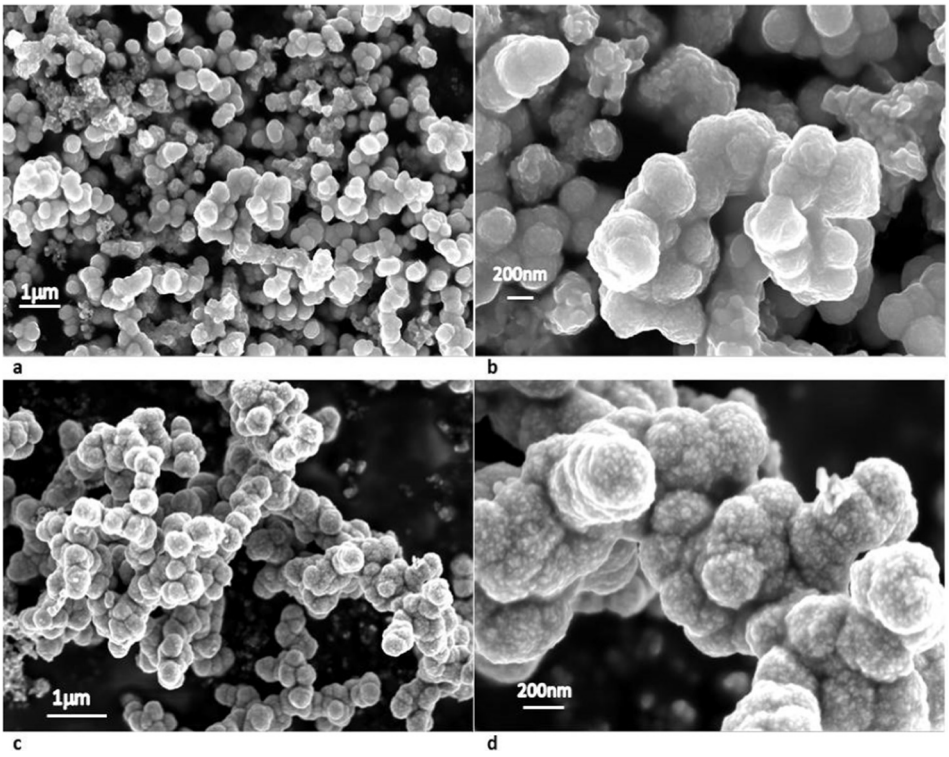

Fig. 2. (a–d) FESEM images of CdS crystals as recycled after CBD.

obtained. Fig. 2d shows the tendency of aggregated nanoparticles to form mesosphere structure. Internal porosity of CdS *meso*-structure can clearly be observed in the figure. Aggregated nanoparticle sizes were measured using FESEM images in Fig. 2(d), and were found to be approximately within the range of 22–90 nm, whereas the size of individual composed sphere is less than a micron (Song and Cölfen, 2010; Fang et al., 2011).

Quantitative elemental analysis of the films was carried out using EDX as shown in Fig. 3 along with the elemental weight and atomic percentage. As shown, the ratio of Cd/S is slightly more than unity which emphasised the presence of sulphur vacancies that act as donors (Saravanan et al., 2011). These results indicate that cadmium sulphide has n-type conduction that makes it suitable for using as window layer in thin film solar cell.

The recycled CdS powder was then used to deposit CdS thin films by thermal evaporation according to the deposition parameters in Table 1. Then they were subjected to different annealing temperatures as mentioned in Table 2 in the hope to achieve suitable recrystallization for practical use. The resultant films were characterized to determine their optical, electrical and structural properties.

The XRD analysis of the thermally evaporated CdS thin films is shown in Fig. 4.

Earlier, all the CdS thin films that were deposited by CBD were found in amorphous nature as Yulisa et al reported. The XRD pattern of

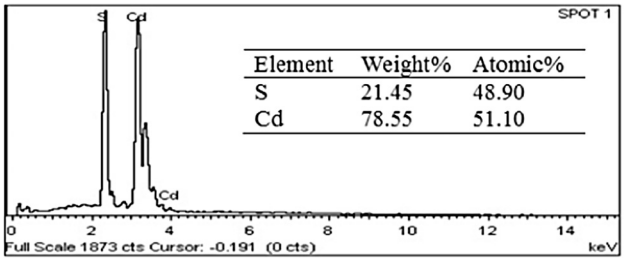

Fig. 3. Elemental composition of produced CdS powder from EDX.

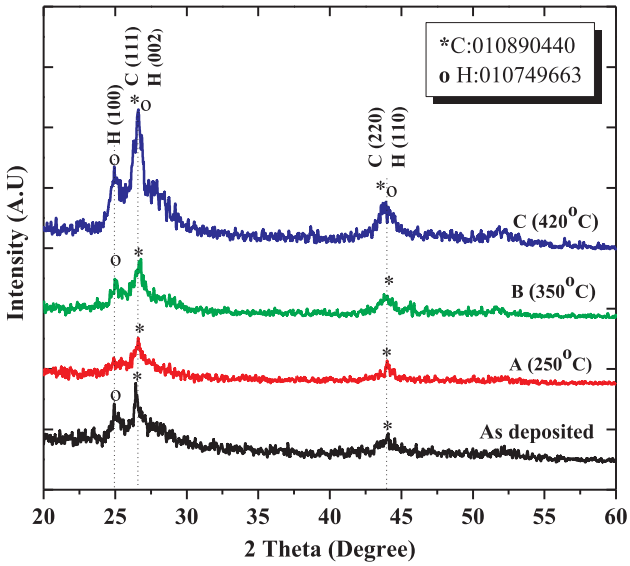

Fig. 4. XRD of CdS thin films at different annealing temperature.

the thermally evaporated CdS thin films show some weak peaks. These peaks suggest that the CdS thin films have mixed hexagonal and cubic phases with preferential orientation in the C(1 1 1) direction. The hexagonal phase almost disappeared for the film annealed at 250 °C and only the cubic phase is observed in Fig. 4 (sample A), which agrees with Zealya et al. who reported that only cubic CdS structure was observed in annealed CdS films at temperatures below 300 °C (Zelaya-Angel and Lozada-Morales, 2000). Hexagonal phase starts to appear clearly at high annealing temperature such as for sample B at 350 °C and more strong at Sample C at 420 °C in contrast with the cubic phase that became weaker, as shown in Fig. 4. Although the XRD patterns of sample C shows mixed hexagonal and cubic structures, other diffraction peaks at (1 0 0) and (1 0 1) of the hexagonal phase have emerged. This may be

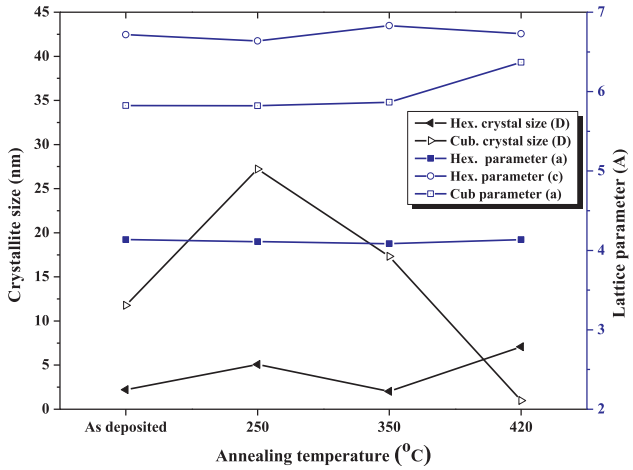

Fig. 5. Crystallite size and lattice parameter of hexagonal and cubic phases of CdS thin films Vs. the annealing temperature.

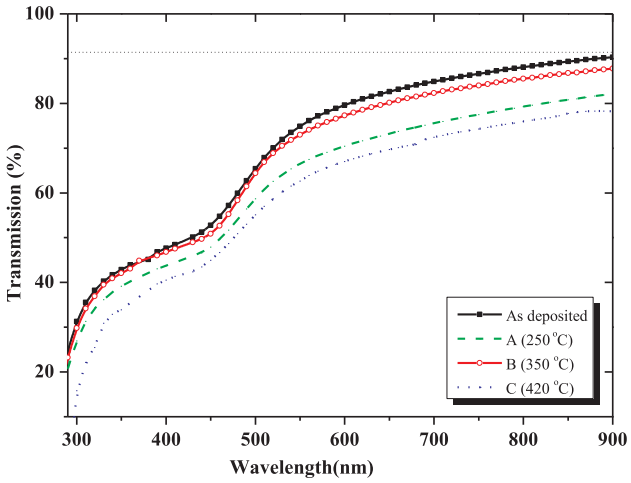

Fig. 7. Transmission spectra for CdS thin films at different annealing temperature.

considered as confirmation on increasing of hexagonal phase as observed in the XRD pattern for the sample C. The peaks as indicated in the JCPDS card no. 01-0749663, at (1 0 0), (0 0 2), (1 0 1) and (1 1 0) of hexagonal phase with space group *P63mc* (1 8 6) and the peaks in JCPDS card no. 01-089-0440 at (1 1 1) and (2 2 0) of cubic phase with space group *F-43m* (2 1 6) were detected. It can be noticed that the positions of the (1 1 1) and (2 2 0) peaks of cubic phase are respectively coincided with (0 0 2) and (1 1 0) peaks of the hexagonal structure of sample C.

Since calculating the crystallite sizes and the lattice parameters is difficult due to the amorphous effect, TOPAS software were therefore used to estimate the lattice parameters and the crystallite size of the cubic and hexagonal phases for the highest peaks, as shown in Fig. 5.

The crystallite size along with hexagonal and cubic phase lattice parameters for CdS thin films were calculated using the TOPAS, as shown in Fig. 5.

CdS thin film grain sizes are ranging between 29 nm and 45 nm, as measured from the FESEM images as shown in Fig. 6. This result confirms that CdS thin films deposited by thermal evaporation normally have small grain sizes (Lee et al., 2003).

The thickness of the films was measured using FESEM, which was found to be around 60 ± 2 nm as shown in Fig. 6. It was expected that the films would have low crystalline structure, as seen in the XRD patterns. Many reasons have been limited the crystallinity such as low deposition temperature, low thickness of the deposited films and deposition on unheated glass substrates (Wakaki et al., 2007; Al-Kuhaili, 2013). FESEM images also show that the films have low voids and no pinholes or cracks.

XRD patterns revealed that heat treatment during annealing

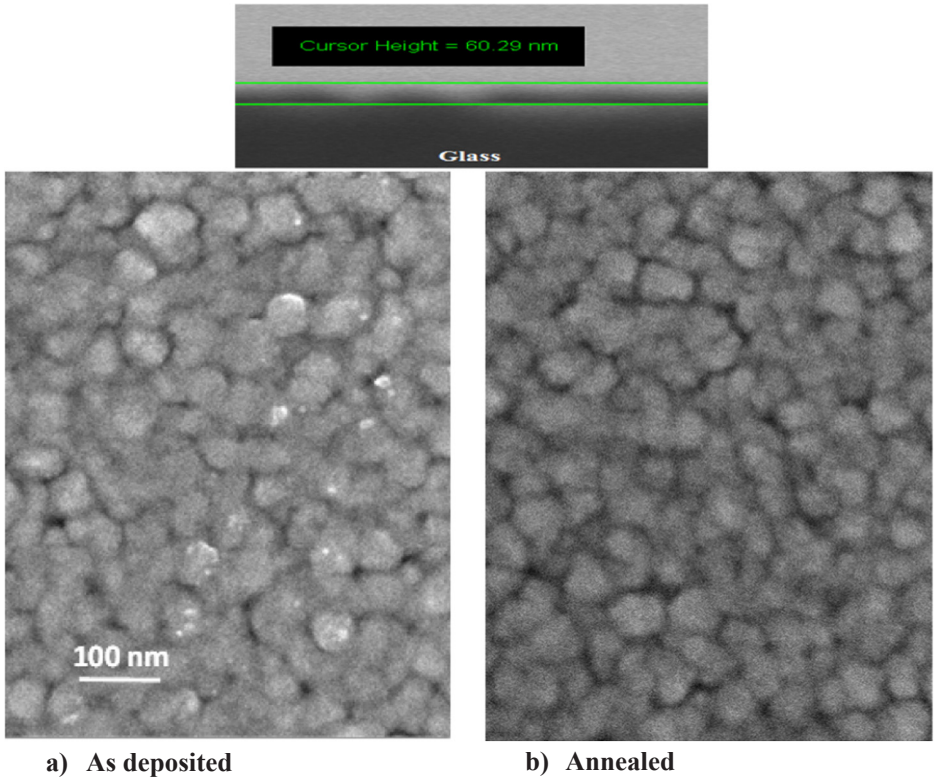

Fig. 6. FESEM images of (a) As-deposited and (b) annealed CdS thin films at 420 °C.

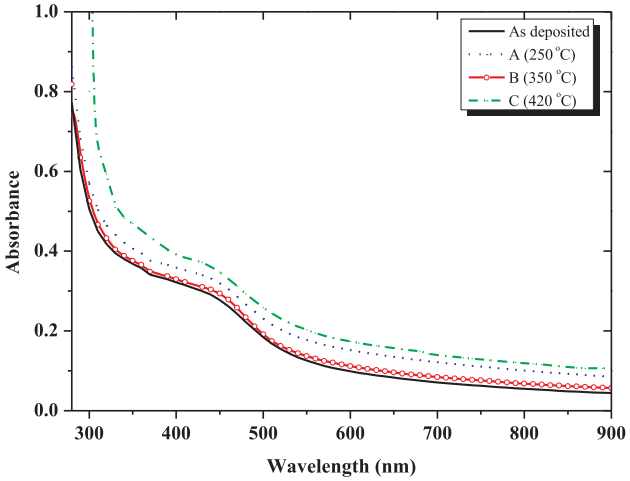

Fig. 8. Absorbance spectra of CdS thin film.

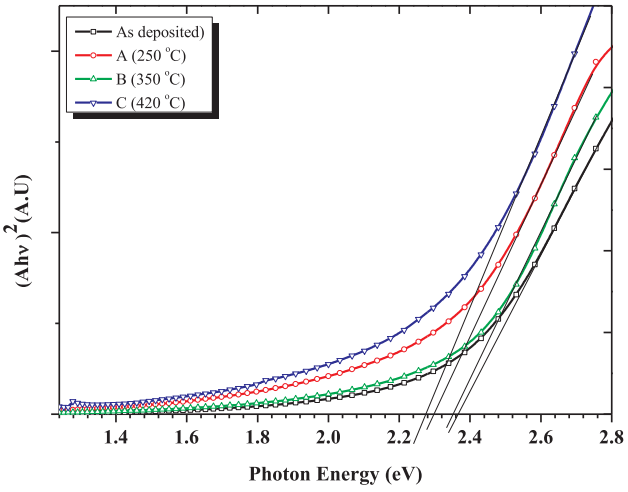

Fig. 9. Extrapolation of bandgap of CdS thin films, as-grown and annealed at different temperature.

Table 4
Energy band gap and Urbach band tail for different CdS thin films.

Sample ID	Band gaps eV	Urbach energy eV
As deposited	2.37	0.57
A	2.30	0.72
B	2.36	0.64
C	2.28	0.76

Table 5
Electrical properties of CdS thin films.

Sample ID	Carrier concentration ($\times 10^{14}$ cm^{-3})	Mobility (cm^2/Vs)	Resistivity (Ω cm) $\times 10^3$
As deposited	2.3	15.7	1.73
A	3.95	9	1.76
B	3.3	4.22	4.49
C	3.34	0.542	34.5

resulted in increased crystallinity of the CdS thin films at temperatures above 400 °C. The hexagonal phase becomes sharp and strong (Ichimura et al., 1999) as can be found in Fig. 4.

Transmission is the most important optical property when CdS thin films are used as window layers in solar cells. Fig. 7 shows the transmission spectra of the CdS thin films. The as-deposited film showed the highest transmittance with the values in between 80% and 90% in the wavelength range 600–900 nm range. Fig. 7 also shows that transmittance decreased when the annealing temperature was increased (A, B, & C).

The same result can be seen from absorption analyses which indicate that the as deposited CdS thin film has the lowest absorbance in visible range. Moreover, the absorption spectra reveals that CdS absorbs the blue region from the visible spectral range (Popescu, 1999), as shown in Fig. 8 below:

The band gap (E_g) can be calculated by plotting a Tauc graph of $(\alpha h\upsilon)^2$ versus the incident photon energy ($h\upsilon$) (Green, 1982), as shown in Fig. 9. The linear nature of the plot confirms that CdS is a direct band gap material.

The Urbach energy E_u associated to the width of the energy tail, exponential-shape tail in curve of Fig. 9, gives information about the thermal disorder or the lattice vibration in crystals. Hence, It is more prominent in amorphous structure than crystalline structure.

The Urbach energy can be determined using the Eq. (4) (Moualkia et al., 2009).

$$\alpha = \alpha_o \exp(h\nu/E_u) \tag{4}$$

where α_o is constant,

The inverse slop of the natural logarithm of absorption coefficient α versus photon energy, using the relation $E_u = [\Delta \ln(\alpha)/\Delta(h\nu)]^{-1}$, the calculated values are given in Table 4.

The as-deposited CdS thin film has an optical band gap of 2.37 eV and this value decreased to 2.30 eV for films annealed at 250 °C, which can be attributed to the cubic single phase that dominated at sample A. While at 350 °C the bandgap increased again to 2.36 eV, however when the annealing temperature was further increased to 420 °C the bandgap decreased abruptly to 2.28 eV. Usually decreasing of CdS bandgap after annealing is attributed to tendency of transition phase from the cubic to hexagonal (Tomas, 1995), this is clear from Fig. 5 which shows decreasing in cubic grains at higher temperature when the hexagonal grains increased. This result is accompanied by amorphous tendency as it can be supported by increasing of the Urbach energy for sample C as in Table 4. Resistivity as well as showing in Table 5 emphasised this result where it started increasing gradually but higher jumped value was at 420C, this may be due to increasing grain boundaries and consequently decreasing the crystallinity. Similar random changes in the bandgap of CdS thin films related to annealing temperature was also reported in many literatures (Zelaya-Angel and Lozada-Morales, 2000; Ichimura et al., 1999; Metin, 2010).

According the data of Table 4, the relation between both energy gap Eg and Urbach energy Eu versus annealing temperature were quadratically fitted.

Obviously, Fig. 10 shows how the increase of energy gap is inversely proportional to the Urbach band tail width.

The quadratic relations for the fitting regression of E_g (eV) and E_u (eV) with T (K) are:

$$E_g = 2.426 - 2.167 \times 10^{-4} T + 5.57 \times 10^{-8} T^2 (eV) \tag{5}$$

$$E_u = 0.366 + 8.37 \times 10^{-4} T - 4.57 \times 10^{-7} T^2 (eV) \tag{6}$$

As the third terms in both equations (5) and (6) are very small, they can be neglected. Then the equation sets become:

$$E_g \approx 2.426 - 2.167 \times 10^{-4} T (eV) \tag{7}$$

$$E_u \approx 0.366 + 8.37 \times 10^{-4} T (eV) \tag{8}$$

This result supports that band gap of most semiconductors decreases with increasing temperature.

Moreover, at low temperature energy gap tends to 2.426 eV, this value has a good agreement with literature value of at 0 K, as shown in Eq. (7) (Böer, 2014). Typically, Second term in Eq. (7) is usually in

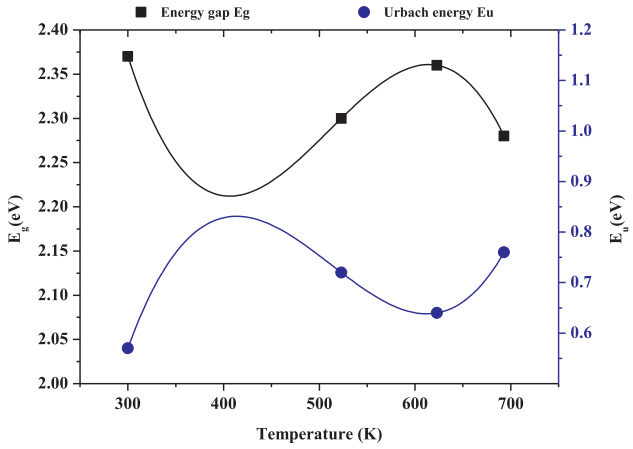

Fig. 10. Energy gap Eg and Urbach energy Eu versus annealing temperature.

order of $-10^{-4}\,eV/K$, result shows a good agreement. This term comes due to the change in lattice vibrations of semiconductor when the electrons jump from the valance band to conduction band. Creating phonons by this vibration leads to a broadening of absorption edge and to the exponential shape; as a result increasing in Urbach energy and energy gap decreasing will be occurred in semiconductors (Kurik, 1971) as clearly describes in Eqs.7 and 8. The Urbach energy falls in range 500 to 800 meV, this is almost agreed with Moualkia (2009). Comparing with CBD CdS thin films reported by Yusoff et al., evaporated CdS thin films showed better properties in term of Urbach energy where CBD films showed higher than 1000 meV (Yusoff, 2015).

Hall Effect measurements were carried out to study the electrical properties, such as carrier concentration, mobility, and resistivity. The results are summarised in the following table.

It is observed that the increase in carrier concentration after annealing is not that high. The carrier concentration is in the order of $10^{14}\,cm^{-3}$ for all samples and these values are in average higher than that concentration of chemical bath deposited CdS films as reported by Yusoff, et al. Mobility decreased drastically whereas resistivity increased with increase in annealing temperature. The causes of this decrease have been suggested to be related with lattice disorder originated by the phase transition.

Khallaf et al. reported similar range of carrier concentration, mobility and resistivity of CdS films (Khallaf, 2008).

4. Conclusion

Recycled CdS powder with mesosphere-like morphology was collected from chemical route using starters from precipitated CBD waste after initial usage for CdS thin film deposition. The collected powder was processed and used to deposit cadmium sulphide (CdS) thin films by simple low vacuum thermal evaporation technique on bare glass substrates, and subsequently annealed at different temperatures. The grown films show properties that make them suitable for the use as window layer in solar cell application. All the films were found to exhibit high transmittance (over 70 to 90%) and low absorbance in the visible/ near infrared region from ~400 nm to 900 nm, thus making it suitable as window layers in solar cells. The optical band gap energy was found to be in the range of 2.28–2.37 eV. Overall this study, the films that were prepared by thermal evaporation methods have better crystallinity and electrical properties than those films prepared by Chemical bath deposition (CBD).

Acknowledgement

The authors would like to acknowledge and appreciate the contribution of The Solar Energy Research Institute of The National University of Malaysia (@UKM) through the research grant with code GUP-2016-042. Due appreciation is also credited to the Institute of Sustainable Energy (ISE) of the Universiti Tenaga Nasional (@The National Energy University) of Malaysia for their support through BOLD2025 Program.

References

Al-Kuhaili, M., et al., 2013. Band gap engineering of zinc selenide thin films through alloying with cadmium telluride. ACS Appl. Mater. Interfaces 5 (11), 5366–5372.
Böer, K.W., 2014. Handbook of the Physics of Thin-film Solar Cells. Springer Science & Business.
BrukerAXS, D.T., 2008. TOPAS 4.2 User Manual. Bruker-AXS GmbH, Karlsruhe, Germany.
Chopra, K., Paulson, P., Dutta, V., 2004. Thin-film solar cells: an overview. Progr. Photovoltaics: Res. Appl. 12 (2–3), 69–92.
Durose, K., Edwards, P., Halliday, D., 1999. Materials aspects of CdTe/CdS solar cells. J. Cryst. Growth 197 (3), 733–742.
Fang, J., Ding, B., Gleiter, H., 2011. Mesocrystals: syntheses in metals and applications. Chem. Soc. Rev. 40 (11), 5347–5360.
Ferekides, C.S., et al., 2000. High efficiency CSS CdTe solar cells. Thin Solid Films 361, 520–526.
Green, M.A., 1982. Solar cells: operating principles, technology, and system applications. Englewood Cliffs, NJ, Prentice-Hall, Inc.
Green, M.A., et al., 2016. Solar cell efficiency tables (version 47). Progr. Photovoltaics: Res. Appl. 24 (1), 3–11.
Guinebretière, R., 2013. X-ray Diffraction by Polycrystalline Materials. John Wiley & Sons.
Ichimura, M., Goto, F., Arai, E., 1999. Structural and optical characterization of CdS films grown by photochemical deposition. J. Appl. Phys. 85 (10), 7411–7417.
Jean, J., et al., 2015. Pathways for solar photovoltaics. Energy Environ. Sci. 8 (4), 1200–1219.
Khallaf, H., et al., 2008. Characterization of CdS thin films grown by chemical bath deposition using four different cadmium sources. Thin Solid Films 516 (21), 7306–7312.
Kurik, M., 1971. Urbach rule. Phys. Status Solidi (a) 8 (1), 9–45.
Lee, J.-H., Lee, D.-J., 2007. Effects of $CdCl_2$ treatment on the properties of CdS films prepared by rf magnetron sputtering. Thin Solid Films 515 (15), 6055–6059.
Lee, J.-H., Lim, D.-G., Yi, J.-S., 2003. Electrical and optical properties of CdTe films prepared by vacuum evaporation with close spacing between source and substrate. Solar Energy Mater. Solar Cells 75 (1), 235–242.
Lisco, F., et al., 2015. The structural properties of CdS deposited by chemical bath deposition and pulsed direct current magnetron sputtering. Thin Solid Films 582, 323–327.
Mariappan, R., et al., 2012. The effect of annealing temperature on structural and optical properties of undoped and Cu doped CdS thin films. Optik-Int. J. Light Electron Opt. 123 (12), 1098–1102.
Martienssen, W., Warlimont, H., 2006. Springer Handbook of Condensed Matter and Materials Data. Springer Science & Business Media.
Metin, H., et al., 2010. Annealing effect on CdS/SnO_2 films grown by chemical bath deposition. Appl. Surf. Sci. 256 (16), 5076–5081.
Morales-Acevedo, A., 2006. Physical basis for the design of CdS/CdTe thin film solar cells. Solar Energy Mater. Solar Cells 90 (6), 678–685.
Moualkia, H., et al., 2009. Growth and physical properties of CdS thin films prepared by chemical bath deposition. J. Phys. D: Appl. Phys. 42 (13), 135404.
Moualkia, H., Hariech, S., Aida, M., 2009. Structural and optical properties of CdS thin films grown by chemical bath deposition. Thin Solid Films 518 (4), 1259–1262.
Oliva, A., et al., 2001. Formation of the band gap energy on CdS thin films growth by two different techniques. Thin Solid Films 391 (1), 28–35.
Pecharsky, V.K., Zavalij, P.Y., 2009. Fundamentals of Powder Diffraction and Structural Characterization of Materials, vol. 69 Springer.
Popescu, V., et al., 1999. Optical properties of cadmium sulfide thin films, chemically deposited from baths containing surfactants. Thin Solid Films 349 (1), 67–70.
Richter, C., Lincot, D., Gueymard, C.A. (Eds.), 2013. Solar Energy. Springer, New York.
Romeo, N., et al., 2004. Recent progress on CdTe/CdS thin film solar cells. Solar Energy 77 (6), 795–801.
Sahay, P., Nath, R., Tewari, S., 2007. Optical properties of thermally evaporated CdS thin films. Cryst. Res. Technol. 42 (3), 275–280.
Saravanan, L., Pandurangan, A., Jayavel, R., 2011. Synthesis of cobalt-doped cadmium sulphide nanocrystals and their optical and magnetic properties. J. Nanoparticle Res. 13 (4), 1621–1628.
Shah, N., et al., 2012. Cu-doping effects on the physical properties of cadmium sulfide thin films. J. Alloys Compd. 512 (1), 185–189.
Song, R.-Q., Cölfen, H., 2010. Mesocrystals: Ordered Nanoparticle Superstructures.
Tao, J., et al., 2016. 7.1% efficient co-electroplated Cu_2 $ZnSnS_4$ thin film solar cells with sputtered CdS buffer layers. Green Chem. 18 (2), 550–557.
Tomas, S., et al., 1995. Influence of thermal annealings in different atmospheres on the band-gap shift and resistivity of CdS thin films. J. Appl. Phys. 78 (4), 2204–2207.
Wakaki, M., Shibuya, T., Kudo, K. (Eds.), 2007. Physical Properties and Data of Optical Materials. CRC Press.
Yusoff, Y., et al., 2015. High quality CdS thin film growth by avoiding anomalies in chemical bath deposition for large area thin film solar cell application. J. Nanosci. Nanotechnol. 15 (11), 9240–9245.
Zelaya-Angel, O., Lozada-Morales, R., 2000. Sphalerite-wurtzite phase transformation in CdS. Phys. Rev. B 62 (19), 13064.